Marine Pollution Bulletin 96 (2015) 110–126

Contents lists available at ScienceDirect

Marine Pollution Bulletin

journal homepage: www.elsevier.com/locate/marpolbul

Intercomparison of oil spill prediction models for accidental blowout scenarios with and without subsea chemical dispersant injection

Scott A. Socolofsky [a,*], E. Eric Adams [b], Michel C. Boufadel [c], Zachary M. Aman [d], Øistein Johansen [e], Wolfgang J. Konkel [f], David Lindo [g], Mads N. Madsen [h], Elizabeth W. North [i], Claire B. Paris [g], Dorte Rasmussen [h], Mark Reed [e], Petter Rønningen [e], Lawrence H. Sim [j], Thomas Uhrenholdt [h], Karl G. Anderson [k], Cortis Cooper [l], Tim J. Nedwed [m]

[a] Division of Coastal and Ocean Engineering, Zachry Department of Civil Engineering, Texas A&M University, 3136 TAMU, College Station, TX 77843-3136, USA
[b] R.M. Parsons Laboratory, Department of Civil and Environmental Engineering, Massachusetts Institute of Technology, Rm. 48-216-B, 15 Vassar Street, Cambridge, MA 02139, USA
[c] Center for Natural Resources Development and Protection, Department of Environmental Engineering, The New Jersey Institute of Technology, Newark, NJ 07102, USA
[d] Centre for Energy, School of Mechanical and Chemical Engineering, University of Western Australia, Crawley, WA, Australia
[e] SINTEF Materials and Chemistry, Environmental Technology, Trondheim, Norway
[f] ExxonMobil Biomedical Sciences, Inc., Annandale, NJ 08801, USA
[g] Rosenstiel School of Marine and Atmospheric Science, Miami, FL 33140, USA
[h] DHI Water and Environment, Hørsholm, Denmark
[i] University of Maryland Center for Environmental Science, Horn Point Laboratory, Cambridge, MD 21613, USA
[j] National Energy Technology Laboratory, U.S. Department of Energy, Albany, OR 97321, USA
[k] Shell Projects & Technology, Houston, TX 77252, USA
[l] Chevron Energy Technology Corporation, San Ramon, CA 94583, USA
[m] Upstream Research Company, Spring, TX 77339, USA

ARTICLE INFO

Article history:
Received 20 January 2015
Revised 12 May 2015
Accepted 13 May 2015
Available online 26 May 2015

Keywords:
Subsea blowout
Droplet size distribution
Chemical dispersant
Model prediction
Multiphase plume
Lagrangian particle tracking

ABSTRACT

We compare oil spill model predictions for a prototype subsea blowout with and without subsea injection of chemical dispersants in deep and shallow water, for high and low gas–oil ratio, and in weak to strong crossflows. Model results are compared for initial oil droplet size distribution, the nearfield plume, and the farfield Lagrangian particle tracking stage of hydrocarbon transport. For the conditions tested (a blowout with oil flow rate of 20,000 bbl/d, about 1/3 of the Deepwater Horizon), the models predict the volume median droplet diameter at the source to range from 0.3 to 6 mm without dispersant and 0.01 to 0.8 mm with dispersant. This reduced droplet size owing to reduced interfacial tension results in a one to two order of magnitude increase in the downstream displacement of the initial oil surfacing zone and may lead to a significant fraction of the spilled oil not reaching the sea surface.

1. Introduction

The Deepwater Horizon accident was the largest oil spill in U.S. waters and the first time that chemical dispersants were applied directly to a leaking wellhead subsea. Dispersants were used to promote smaller oil droplet sizes, which may have led to longer residence times in the water column. This is consistent with improved air quality witnessed in the response zone directly above the wellhead when dispersants were applied subsea: oil likely surfaced farther downstream, away from the wellhead response, and more oil may have been degraded subsurface. On the other hand, these apparent benefits of dispersant application come with different ecosystem effects, which depends on the fate and transport of the oil in treated and untreated cases. Thus, as part of the planning for mitigation of future events, it is critical to understand how oil transport is affected by subsea dispersant injection and how well the transport is represented in oil spill models.

* Corresponding author.
E-mail addresses: socolofs@tamu.edu (S.A. Socolofsky), eeadams@mit.edu (E.E. Adams), boufadel@gmail.com (M.C. Boufadel), zachary.aman@uwa.edu.au (Z.M. Aman), oeis-joh@online.no (Ø. Johansen), wolfgang.j.konkel@exxonmobil.com (W.J. Konkel), dlindo@rsmas.miami.edu (D. Lindo), mm@dhigroup.com (M.N. Madsen), enorth@umces.edu (E.W. North), cparis@rsmas.miami.edu (C.B. Paris), dor@dhigroup.com (D. Rasmussen), Mark.Reed@sintef.no (M. Reed), Petter.Ronningen@sintef.no (P. Rønningen), Lawrence.Sim@contr.netl.doe.gov (L.H. Sim), thu@dhigroup.com (T. Uhrenholdt), karl.g.anderson@shell.com (K.G. Anderson), cortcooper@chevron.com (C. Cooper), tim.j.nedwed@exxonmobil.com (T.J. Nedwed).

http://dx.doi.org/10.1016/j.marpolbul.2015.05.039
0025-326X/

During a spill event, much of the decision-making process is driven by predictions from integrated spill prediction models. After a spill, these and research-oriented models provide critical insight on what the ecosystem effects may have been. In either case, the sequence of processes post release is commonly handled by three modeling components. The initial jet breakup into gas bubbles and oil droplets is believed to occur very close to the source, and is simulated by a droplet size distribution (DSD) model, either based on empirical equilibrium equations (e.g., Johansen et al., 2013) or dynamic population evolution models (e.g., Bandara and Yapa, 2011; Zhao et al., 2014a). The jet of oil and gas leaves the breakup region as a coherent plume, which entrains ambient water and can be efficiently modeled using a buoyant jet integral model similar to sewage outfall plumes (e.g., Jirka, 2004; Lee and Chu, 2003), but adapted to account for the multiphase dynamics of oil and gas (e.g., Johansen, 2000, 2003; Zheng et al., 2003). Due to the ambient density gradient in the oceans, the buoyant jet is arrested as it rises through the water column, and one or more intrusion layers form. These intrusion layers contain detrained seawater, dissolved hydrocarbons, and, potentially, small oil droplets. It is not well known how bubbles or droplets are transported immediately above the intrusion layers, but eventually they are expected to transition to a Lagrangian particle (droplet and bubble) transport phase in the farfield, where group buoyancy effects and plume dynamics are negligible. The purpose of the study described in this paper is to inter-compare the predictions from a suite of available blowout models for a range of prescribed test cases in shallow and deep water with and without subsea chemical dispersant application. The definition of a benchmark set of tests is necessary for the intercomparison exercise, and these tests cases will remain useful for future model development, where new and developing models can be compared to the results presented here. The model intercomparison itself is helpful to understand the variability that can be expected among model predictions for similar spills. Sources of variability result from differences in model formulation and different choices made by the modelers for the same set of input data. The study also contributes to an evaluation of potential dispersant effectiveness across the range of test cases.

Laboratory experiments for multiphase plumes in stratification and crossflow highlight some of the general features of blowout plumes in the oceans. Fig. 1 shows dye visualization experiments for bubble plumes in pure stratification, pure crossflow, and the combined effects of stratification and crossflow. In pure density stratification (Fig. 1a), entrained seawater rises with the bubbles until the drag from the bubbles cannot lift the heavy seawater any higher, and the seawater detrains from the plume at a peel height h_p. The detrained fluid descends along an outer ring surrounding the rising bubble column, and comes to rest at a height of neutral buoyancy, forming an intrusion layer at the trap height h_T. Asaeda and Imberger (1993) observed this behavior for lake aeration plumes, and their paper forms the basis of double-plume integral models used to capture both the inner and outer plume formation and the multiple intrusion layers that can form. Fig. 1a shows the lowest intrusion layer, but in the absence of crossflow, this process repeats itself throughout the water column (see e.g., Socolofsky et al., 2008). This behavior of multiple intrusions was also observed during the Deepwater Horizon blowout (Valentine et al., 2010; Socolofsky et al., 2011; Paris et al., 2012; Spier et al., 2013), with the dominant intrusions centered on 1100 m and 800 m depth. Fig. 1b shows the classic behavior in pure crossflow. Entrained water rises with the bubbles until a separation height h_S, above which the bubbles rise independently from the separated plume. In the figure, the separated plume is a single-phase jet of water and dye; for a blowout, the separated plume contains dissolved hydrocarbons and could also contain smaller oil droplets

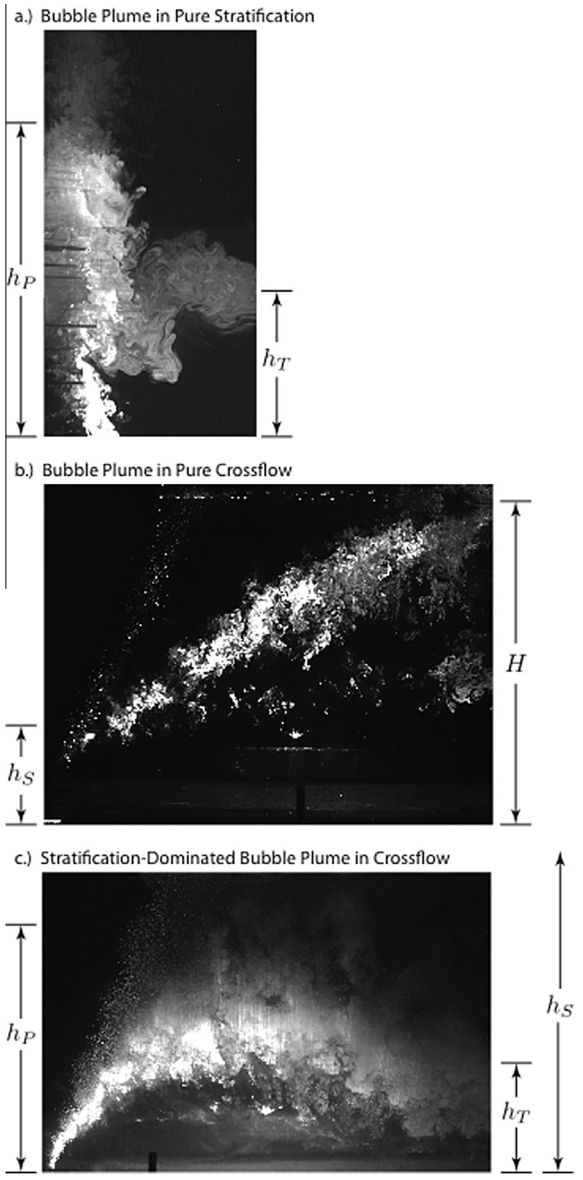

Fig. 1. Dye visualization of bubble plumes in laboratory experiments for (a) pure stratification with no crossflow (h_S = infinity) (adapted from Seol et al. (2009)), (b) pure crossflow with no stratification (h_P = infinity), and (c) combined effects of stratification and crossflow for a stratification-dominated plume ($h_P < h_S$).

(see e.g., Socolofsky and Adams, 2002). Fig. 1c shows an example of the combined effects of stratification and crossflow. For this experiment, the density stratification, crossflow velocity, and bubble flow rate is set so that the separation height h_S is much greater than the peel height h_P. The detrained fluid descends due to its negative buoyancy, which is very different from the behavior in Fig. 1b, where the neutrally buoyant dye continues to rise due to the excess momentum imparted to it by the bubble column prior to separation. In the stratified case, the separated dye eventually oscillates about the neutral buoyancy level, close to the prediction for h_T in pure stratification.

The only available field experimental data of blowout plumes are from the DeepSpill experiment (see e.g., Johansen et al., 2003). This experiment had a buoyancy flux ~1/10 that of the Deepwater Horizon blowout and was conducted at a site with weaker stratification and stronger crossflows. For that experiment, h_S was generally less than h_P, and the plume could be classified as crossflow dominated, similar in appearance to Fig. 1c, but with the

separation occurring because of the crossflow rather than the stratification. Lagrangian plume models calibrated to the crossflow separation data in pure crossflows in Socolofsky and Adams (2002) agree well with the trajectories measured during the field experiment (Chen and Yapa, 2003; Johansen, 2003). During these experiments multiple subsurface intrusions were not observed due to the strong crossflow, and most mainstream blowout models are based on single-intrusion algorithms as in the Chen and Yapa (2003) CDOG and Johansen (2003) DeepBlow models.

To compare the range of predictions from available blowout models and effect of subsea dispersant application as predicted by these models, a model intercomparison exercise was sponsored by the American Petroleum Institute (API) through the Joint Industry Task Force, D3 Subsea Dispersant Injection Modeling Team, with co-sponsorship by the BP/Gulf of Mexico Research Initiative through the Gulf Integrated Spill Research (GISR) and Center for Integrated Modeling and Assessment of the Gulf Ecosystem (C-IMAGE) consortia. Modelers were given a matrix of test cases, described in Section 2 below, and asked to present their modeling results at a Workshop conducted in Houston, Texas, USA, on January 31, 2014. The models were run by their developers or experienced users, and representatives from each modeling group are included in the author list of this paper. The participating models were:

- The SINTEF Oil Spill Contingency and Response (OSCAR) model, which includes the DeepBlow model as the integrated nearfield plume model, Plume-3D.
- The National Energy Technology Laboratory (NETL) Blowout and Spill Occurrence Model (BLOSOM).
- The MIKE by DHI Oil Spill (OS) module, with integrated nearfield plume model and coupled Lagrangian and Eulerian model for tracking of dispersed and dissolved oil in the farfield.
- RPS ASA's oil spill model OILMAP, which includes the OILMAPDeep module as the integrated near-field plume model, was utilized as part of this study. OILMAP's far-field module was not used; instead simple surfacing calculations using analytical solutions were performed.
- A hybrid modeling approach of empirical and Lagrangian particle tracking models. Empirical correlation equation models were applied for the initial bubble and droplet break-up (using equations in Johansen et al., 2013) and the nearfield plume dynamics (following Socolofsky et al., 2011). These results were provided as initial conditions to two different research-oriented farfield transport models, the Lagrangian Transport (LTRANS) model, run by coauthor North from the University of Maryland, and the Connectivity Modeling System (CMS), run by coauthor Paris from the Rosenstiel School for Marine and Atmospheric Science.

These models span a range of well-developed and new modeling systems, both from industry and academia. Several other mainstream and research model teams were invited. Because all models were run *pro bono* and the dates of the intercomparison workshop were fixed, not all invitees could participate. The analysis team of coauthors Socolofsky, Adams, and Boufadel performed the intercomparison of the model results provided by the teams listed.

This paper describes the main features of this subset of models and presents an analysis of their predictions for a comprehensive test suite of accidents in deep and shallow water with and without subsea dispersant injection defined in this model intercomparison. Section 2 defines the test cases used in the API Model Intercomparison. These cases specify the input data used by all models and provide the information needed by future model developers to compare their results to the benchmark results presented here. A summary of the algorithms used and the results for the droplet size distribution from the intercomparison exercise are presented in Section 3. The nearfield plume intercomparison metrics and results are given in Section 4, followed in Section 5 by the farfield Lagrangian particle tracking metrics and results. Section 6 summarizes the main findings and suggests areas for future model development and needed additional validation data.

2. Model intercomparison test data

The model intercomparison tests are designed to study differences in the fate of oil spilled from a range of potential blowout conditions. A critical aspect of the study is to understand how the model predictions change when adding chemical dispersants at the spill source, as was done during the Deepwater Horizon accident. Adding dispersants is expected to reduce the oil droplet size, helping to keep the oil suspended in the water column. If effective, this has the dual effect of sequestering the oil away from contact with responders and likely promoting more rapid dissolution and biodegradation of the oil due to the higher surface area of small droplets compared to larger droplets. Thus, it is important for the models to predict both the initial droplet size distribution as well as the fate of the oil in the water column for the intercomparison.

To interpret the range of predictions for a set of models, it is necessary to minimize differences in the input data used by each model without constraining their various solution schemes. Specifying the initial conditions just upstream of the release point and conducting the intercomparison exercise in two phases accomplishes this. The release conditions include detailed flow rates, accident release geometry and depth, composition of the spilled oil and gas at the release, and the dispersant-to-oil ratio. In phase 1, modelers were asked to predict the initial bubble and droplet size distributions from the provided initial conditions. The results of phase 1 were submitted to API and analyzed ahead of the plume and farfield predictions conducted in phase 2. After reviewing the range of methodologies and predictions for the droplet and bubble size distributions, API released a consensus bubble and droplet size distribution to be used in a subset of the test cases (case 1 through 8 and 13 and 14) in phase 2. For these cases, differences in the solution schemes used by each plume and farfield model could be assessed independent of differences in predicted droplet size distributions. For the other cases (9 through 12) solutions for the droplet and bubble size distributions predicted by each modeling team in Phase 1 were also studied. Hence, in all, 14 test cases were defined for the intercomparison. These cases are summarized in Table 1, which includes the API-specified droplet sizes following the analysis of phase 1; bubble sizes were specified at 10 mm diameter for these cases.

Several initial conditions are held constant across all cases. The oil flow rate is fixed at 20,000 bpd of oil, which is about 1/3 the flow rate estimated for the Deepwater Horizon (McNutt et al., 2011). The exit temperature is 150 °C at the release point, and the oil and gas are spilled through a circular orifice of 0.3 m diameter. The dispersant addition was assumed to be efficient, at a dispersant to oil ratio (DOR) of 2%, but it was left to the modelers to decide on the resulting reduction in interfacial tension; most modelers assumed a 200 fold reduction following Brandvik et al. (2013b). A single model of a light, sweet crude with very little carbon dioxide or sulfur dioxide was chosen for the oil. While the 20,000 bpd flow rate gives a constant mole flux of the oil components for all simulations, the composition of the gas and liquid phases and their mole fractions for each depth and GOR combination are different.

In order that all modelers handle the oil state in the same way, the equilibrium gas and oil composition was computed from the MultiFlash™ program by Infochem Software

Table 1
Test matrix defining the 14 model runs in the intercomparison. GOR is gas to oil ratio at surface conditions, U_a is the ambient current velocity, DOR is the dispersant to oil ratio at the subsurface injection, and d_{50} is the volume median diameter of oil droplets at the source.

Case	Depth (m)	GOR (std ft^3/bbl)	U_a (m/s)	DOR (%)	d_{50} (mm)
1. Deep base case	2000	2000	0.05	0	3.8
2. Deep base case with dispersant	2000	2000	0.05	2	0.20
3. Deep case with low GOR	2000	500	0.05	0	3.9
4. Deep case with low GOR and dispersant	2000	500	0.05	2	0.41
5. Shallow base case	200	2000	0.05	0	2.6
6. Shallow base case with dispersant	200	2000	0.05	2	0.41
7. Deep case with high ocean current	2000	2000	0.3	0	3.8
8. Deep case with high ocean current and dispersant	2000	2000	0.3	2	0.2
9. Deep base case with modeler's DSD	2000	2000	0.05	0	Modeler
10. Deep base case with dispersant and modeler's DSD	2000	2000	0.05	2	Modeler
11. Shallow base case with modeler's DSD	200	2000	0.05	0	Modeler
12. Sallow base case with dispersant and modeler's DSD	200	2000	0.05	2	Modeler
13. Deep base case with no oil degradation (no dissolution or biological processes)	2000	2000	0.05	0	3.8
14. Deep base case with no oil degradation with dispersant	2000	2000	0.05	2	0.20

(http://www.kbcat.com/infochem-software/flow-assurance-software-multiflash) and the results were provided to each modeler. Table 2 gives the gas and oil composition by component in mole fraction for the three different combinations of depth and GOR used in the test matrix of Table 1. These conditions represent the oil and gas in thermodynamic equilibrium with each other at the release conditions. For the deeper cases, there is a significant fraction of light components dissolved in the liquid phase. Several bulk properties of the gas and liquid phases along with their mass fluxes at the release were also specified. These are presented in Table 3, giving the properties of live oil released at the wellhead. These values are much different from the typical dead oil properties in the model databases, and these live oil properties, especially the low density and low viscosity resulting from the high amount of dissolved methane, play a significant role in the blowout dynamics.

The lateral boundary conditions for the models are given by the ambient water column data. Since the focus of the study is on assessing differences in the predictions of these models for water column fate, it was elected to have an unbounded domain of constant water depth and to use a single profile of salinity and temperature with a uniform velocity over the depth for all cases. The salinity and temperature profile is the global mean profile reported in Sarmiento and Gruber (2006), which uses the data from Levitus et al. (1998), shown in Fig. 2. It is necessary for temperature and salinity to vary with depth in order to preserve the density stratification of the ocean. The buoyancy frequency given by this profile is 0.0015 s^{-1} at 2000 m depth, increasing approximately linearly to 0.003 s^{-1} at ~500 m depth, and then rapidly increasing to 0.01 s^{-1} at the surface. The oxygen profile is provided in the case that gas stripping is modeled in the simulations. The velocity profile was chosen to be constant to keep the simulation conditions as simple as possible.

Table 3
Bulk properties and mass flow rates of the gas and liquid phases for the three different release conditions in the intercomparison test matrix. H is the water depth and GOR is the gas to oil ratio at surface conditions in std ft^3/bbl.

Bulk Property	H = 2000 m GOR = 2000		H = 2000 m GOR = 500		H = 200 m GOR = 2000	
	Gas	Liquid	Gas	Liquid	Gas	Liquid
Density (kg/m^3)	131.8	599.3	–	649.9	13.5	718.5
Interfacial tension (N/m)	0.06	0.015	–	0.015	0.06	0.015
Dynamic viscosity (Pa s)	2e−5	2e−4	–	2e−4	2e−5	2e−4
Mass flux (kg/s)	7.4	34.5	–	32.6	12.7	29.2

Although these data fully describe the release conditions, not all models used the same initial conditions for the simulations presented below. The main source of discrepancy depended on how the models specified the gas and oil composition and flow rate for their simulations. The simplified method used by most models is to specify the oil flow rate and GOR at standard conditions along with a compressibility model for the equation-of-state. Gas is typically modeled by its main component, and compressed using a real gas equation-of-state, such as the Peng-Robinson cubic equation-of-state (McCain, 1990). Oil is either treated as incompressible, or modeled by a simplified equation-of-state. For example, an equation of state in McCain (1990) uses the API gravity and the thermal expansion and isothermal compressibility coefficients

Table 2
Mole fractions of constituents of gas and liquid oil for the three different release conditions in the intercomparison test matrix. H is the water depth and GOR is the gas to oil ratio at surface conditions in std ft^3/bbl.

Component	H = 2000 m GOR = 2000		H = 2000 m GOR = 500		H = 200 m GOR = 2000	
	Gas	Liquid	Gas	Liquid	Gas	Liquid
Carbon dioxide	0.000822	0.000591	0	0.000430	0.000881	0.0000970
Nitrogen	0.00403	0.00132	0	0.00156	0.00335	0.000105
Methane	0.617	0.424	0	0.372	0.788	0.0505
Ethane	0.0640	0.0585	0	0.0396	0.0796	0.0121
Propane	0.0439	0.0471	0	0.0296	0.0526	0.0150
i-Butane	0.00960	0.0113	0	0.00750	0.0110	0.00493
n-Butane	0.0220	0.0271	0	0.0188	0.0246	0.0134
i-Pentane	0.0100	0.0136	0	0.0115	0.0101	0.00971
n-Pentane	0.0121	0.0168	0	0.0155	0.0118	0.0130
Hexane	0.0211	0.0326	0	0.0383	0.0158	0.0388
C7+[a]	0.197	0.367	0	0.466	0.00278	0.842

[a] The thermodynamic properties of C7+ are: molecular weight = 200 g/mol, critical point temperature = 705.26 K, critical point pressure = 1,766,920 Pa, acentric factor = 0.64751, boiling temperature = 531.15 K, and specific gravity = 0.813 at standard conditions.

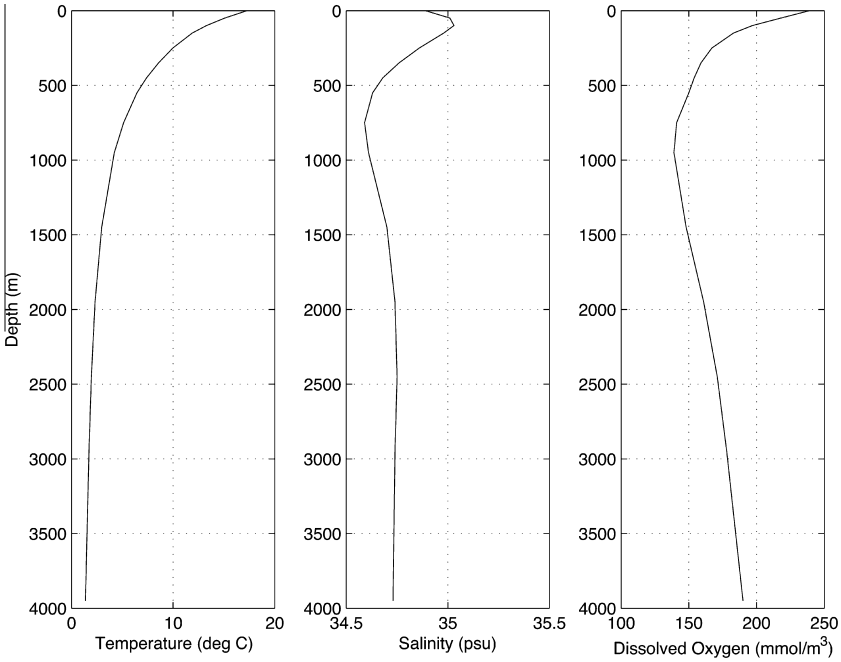

Fig. 2. Profiles of ambient ocean properties. Data taken from Sarmiento and Gruber (2006).

to account for temperature and pressure changes. This method of specifying the flow rates explicitly ignores the equilibrium partitioning of the gas in the oil at depth and assumes all gas is released from the well as free gas. Because this assumption is inconsistent with the equation of state specified in Tables 2 and 3, such an alternative model was not provided to the modelers for the intercomparison. Moreover, models would not be able to consistently predict the dissolution or biodegradation of oil if the composition were not specified. Some of the models do use pseudo-component equations-of-state such as those in the tables; however, because the modeling was done *pro bono*, none of the teams afforded the time to add the specified oil to their simulation tool, but rather selected a similar oil already in their model's database. These facts resulted in each modeling team using a slightly different mass flux and density of gas and oil at the release than specified in the tables. The slight differences result in different predictions for the oil droplet size, and ultimately, different predictions for the oil fate. These differences are explored in detail in Section 3, below.

While it would have been ideal for each model to exactly use the oil specified above, this exercise is still more constrained than what can be expected early on during an actual emergency, when the flow rate, GOR, spill geometry, and even spill depth may not be well known. In addition, even for models that release oil with significant dissolved methane fraction, there are no data in the literature documenting the mechanisms for how methane leaves the liquid phase as pressure is relieved during transit to the surface. Hence, the results presented below have much lower differences in their initial conditions than the uncertainty that will be present during a real event, and most of the model variability in the results can be attributed to different choices in the model algorithms and solution schemes.

3. Droplet size distribution

3.1. Breakup models

There are two basic approaches available to predict droplet size distribution from jet breakup. These are equilibrium models, which predict a characteristic stable droplet size after breakup evolution has ended (e.g., Hinze, 1955; Johansen et al., 2013; Wang and Calabrese, 1986), and population dynamic models, which take a seed droplet size and model the time-evolving breakup and coalescence processes using force and mass balance equations (e.g., Bandara and Yapa, 2011; Tsouris and Tavlarides, 1995; Zhao et al., 2014b). Of the models included in the intercomparison, all use the equilibrium modeling approach. We also present results from the population dynamics model VDROP-J described in Zhao et al. (2014b) for comparison.

Most equilibrium models assume that droplet size depends on a balance between the restoring force of interfacial tension σ and breakup forces, which for a jet are dominated by turbulence, characterized by the jet's energy dissipation rate ε. Because ε is in energy per unit weight, the density ρ enters the dimensional analysis. With these parameters, a characteristic droplet size d scales with

$$d \propto \left(\frac{\sigma}{\rho}\right)^{3/5} \varepsilon^{-2/5}$$

For a jet, the dissipation rate scales with the centerline velocity and jet half-width, which, near the point of release, scale with the jet exit velocity U and orifice diameter D, giving

$$\varepsilon \propto \frac{U^3}{D}$$

Combining these results gives a predictive equation for the droplet size distribution after breakup in a jet given by

$$\frac{d_n}{D} = A_n \left(\frac{\rho U^2 D}{\sigma}\right)^{-3/5} = A_n We^{-3/5} \tag{1}$$

where We is the Weber number. The proportionality coefficient A_n is determined by comparison to experimental data, and depends on the selection of the characteristics droplet size d_n, where n% of the distribution is in sizes smaller than d_n. For example, d_{50} is the volume median diameter. In general, size distributions can be given on a volume (or mass) basis or a number basis. We use d_n for volume distributions and substitute δ_n for the characteristic diameter for a number distribution.

One complication in applying this model is selection of the density in the Weber number. Jet break-up is a multiphase process, and either the density of the continuous (receiving) phase or of the dispersed phase (the phase undergoing breakup) can be used. A survey of the chemical engineering literature indicates that some authors use the continuous phase, while others use the dispersed phase density in the definition of *We*. This choice is important when comparing to experimental results or predicting field cases as gas density is generally at least an order of magnitude less than water and live oil density can also be as low as half that of water. Each of the models presented here applies a *We* definition chosen by the modeler, and both options are represented in the results. In any case, care must be taken that the value chosen for A_n is consistent with the definition of the Weber number used when A_n was calibrated.

Data for oil jet breakup with dispersants also uncovers an additional limiting force for the droplet size distribution. Dispersants lower the interfacial tension σ, and when σ is low, the Weber number becomes large, and increasingly smaller droplet sizes are predicted by Eq. (1). In contrast, experiments by Brandvik et al. (2013b) and Belore (2014) show that droplet size does not continue to decrease with decreasing surface tension when high levels of dispersant are used in a jet breakup test of oil. This is consistent with observations by Wang and Calabrese (1986), who showed that viscosity begins to limit breakup as interfacial tension becomes small. The effect of viscosity can be accounted for by more than one non-dimensional number, including the Reynolds, Ohnesorge, or Viscosity numbers. Wang and Calabrese (1986) propose using the Viscosity number

$$Vi = \frac{\mu_p U}{\sigma}$$

where μ_p is the dynamic viscosity of the dispersed phase fluid to account for this behavior. Johansen et al. (2013) apply this approach and define a modified Weber number that incorporates the viscosity number. When compared to the data of Brandvik et al. (2013b), the resulting equilibrium model becomes

$$\frac{d_n}{D} = A_n \left[\frac{We}{1 + B_n Vi (d_n/D)^{1/3}} \right]^{-3/5} = A_n We^{*-3/5} \tag{2}$$

where B_n is an empirically-derived model coefficient and We^* is the modified Weber number. The model is implicit for the characteristic droplet size d_n when B_n is not zero. Also, note that the calibration parameter B_n is contained in the definition of We^*.

Both models (Eqs. (1) and (2)) predict one characteristic size of the droplet distribution. To predict the remainder of the droplet size distribution, a probability density function and spread coefficient values are needed. All but one of the models presented in the intercomparison use the Rosin–Rammler distribution, given by

$$V(d) = 1 - \exp\left(-\ln\left(\frac{n}{100}\right) \left(\frac{d}{d_n}\right)^{\alpha} \right) \tag{3}$$

where α is a spread coefficient. The other model uses the derived distribution defined in Chen and Yapa (2007) which has similar shape, but is derived from a theoretical basis.

For certain spill conditions, the above models may produce unrealistically large bubble or droplet sizes. To correct for this, some modelers set a fixed maximum allowable size. An alternative is the simple equation for maximum stable droplet size from Clift et al. (1978), given by

$$d_{\max} = 4\sqrt{\frac{\sigma}{g(\rho - \rho_p)}} \tag{4}$$

where g is the acceleration of gravity and ρ and ρ_p are the densities of the continuous and dispersed phase, respectively.

Almost all of the data available to calibrate the model coefficients A_n, B_n, and α for breakup in a jet are based on experiments with a single dispersed phase, generally oil or gas. For the intercomparison cases, as well as most real world scenarios, there is a discharge of both oil and gas, and a choice needs to be made how to select the effective exit diameter D and discharge velocity U since the flow will be comprised of a mixture of oil and gas and the droplet size for each phase is sought separately. Johansen et al. (2013) present a method to increase the momentum of the exiting oil by accounting for the restricted cross-sectional area of the orifice caused by the presence of the gas. The momentum is also assumed to increase, compared with a pure jet, due to the buoyancy flux of the gas. Other methods use the superficial velocity or neglect the influence of the added phase and move the effect to the fit parameters. In each case, the corrections are theoretical, as there are too few reliable measurements in the literature for mixed phase plumes to use as calibration data.

Table 4 lists the characteristic droplet size, proportionality coefficients, and density used in the Weber number for each of the models included in the intercomparison.

3.2. Sensitivity of breakup models

As pointed out in Section 2, none of the modeling teams used the exact oil properties specified in the intercomparison matrix, but rather used oil properties convenient to their model and similar to those provided. This influences the prediction of droplet size distribution through the exit velocity U, which depends on the density and mass flux of the spilled fluids. In this section, we focus on the Johansen et al. (2013) model (Eq. (2), above) and present a sensitivity analysis to oil type and also to the model fit coefficients.

Results for the OSCAR model using Eq. (2) and the fit parameters in Johansen et al. (2013) were submitted by SINTEF for phase 1 of the model intercomparison exercise. They chose to use the pre-defined model oil in OSCAR called Sleipner, which has a specific gravity of 0.745 and viscosity of $1 \cdot 10^{-3}$ Pa s. This is a light oil with dynamic viscosity about five times higher than the specified oil. For comparison here, we use Eq. (2) with the oil properties specified in Section 2 with two sets of coefficients A_n and B_n. In one set of calculations, we use the fit parameters in Johansen et al. (2013), $A_{50} = 15$ and $B_{50} = 0.8$, and in the second set of calculations, we use $A_{50} = 24.8$ and $B_{50} = 0.08$. The later set of coefficient values was determined by SINTEF in work for API based on a more comprehensive dataset of oil jet breakup experiments with and without dispersant (Brandvik et al., 2013a). In all the results presented here, the interfacial tension is reduced by a factor of 200 when chemical dispersants are applied. This interfacial tension reduction factor is consistent with SINTEF breakup experiments using Corexit 9500 at DOR of 2%.

Table 4
Parameter choices for the droplet size distribution prediction. Parameters d_n, A_n, and B_n, are defined in Eq. (2), α is defined in Eq. (3), ρ is the density of seawater, ρ_p is the density of oil, and *We*, is the Weber number, defined in Eq. (1).

Model	d_n	A_n	B_n	α	ρ in *We*
OSCAR	d_{50}	24.8	0.08	1.8	ρ_p
MIKE	d_{50}	15	0.8	1.8	ρ_p
BLOSOM	$d_{\max}$	20 if GOR[a] ⩽ 19 4 if GOR[a] > 19	0	1.6 if GOR[a] ⩽ 19 2.5 if GOR[a] > 19	ρ if GOR[a] ⩽ 19 ρ_p if GOR[a] > 19
RSMAS	d_{50}	0.063	0.016	1.8	ρ_p
OILMAP Deep	d_{95}	20	0	1.6	ρ

[a] GOR is the gas to oil ratio (dimensionless) at the release point and not at standard conditions.

Fig. 3 presents the results of the OSCAR predictions using the Sleipner oil and those using the oil specified in the API intercomparison. The open circles for the API-specified oil results are plotted for the model coefficients in Johansen et al. (2013) (A_{50} = 15 and B_{50} = 0.8); the error bars represent the range using those coefficients (the lower range of the error bar) or using the latter coefficients A_{50} = 24.8 and B_{50} = 0.08 (the upper range of the error bar). The maximum stable droplet size is predicted from Eq. (4) using the properties of the API-specified oil. In the deep cases (1–4), the volume flow rates are lower due to the compressibility of the gas, and the droplet sizes are larger compared to the shallow cases (5 and 6). For the API-specified oil, the droplet sizes exceed the maximum stable size when using A_{50} = 24.8 and B_{50} = 0.08 for cases 1 and 3. In the shallow case (5) with high exit velocity, and in all the cases with applied dispersant (2 and 4), the absolute magnitude of the difference among the various model results is lower than in the deeper, no-dispersant cases (1 and 3). Also, the range of predictions using the two sets of model coefficients is generally greater than the variability between the models using different oils.

In order to characterize the spread in predicted droplet size when using the same model with varying oil type or model coefficients, or in the following section when using different models, we use the coefficient of variation, CV, defined as

$$\mathrm{CV} = \frac{1}{\mu}\sqrt{\frac{\sum_1^n (x_i - \mu)^2}{(n-1)}} \tag{5}$$

where x_i represents a predicted value and μ is the mean of the predicted values. Eq. (5) uses $n - 1$, rather than n, to provide an unbiased estimate of the spread in predicted values based on the (larger) population of all model predictions. In comparing model predictions with only two oil types or two sets of coefficients, n = 2, and the CV becomes $2^{1/2}(H - L)/(H + L)$, where H and L refer to the higher and lower model prediction. For the API specified oil using the two sets of coefficient values, the CVs are 35%, 20%, 35%, 23%, 34%, and 16% for cases 1–6, with an average of 35% for the no-dispersant cases, an average of 19% for the dispersant cases, and an overall average of 27%. Because the experiments used to calibrate the two sets of coefficients were conducted by the same research team, under similar conditions, and using the same oil, the CV of 27% reflects the average baseline (minimum) uncertainty one might expect from current models. Meanwhile, using the Johansen et al. (2013) coefficient values, the CV for the two types of oil are 25%, 25%, 47%, 1%, 6%, and 22% for cases 1–6, with an average of 21%. These differences are similar to those due to the model coefficients, and reflect the uncertainty one might expect by making predictions for an oil with slightly different properties.

To explore the sensitivity of the model predictions from Eq. (2) to other input variables, a second sensitivity analysis was performed for the test matrix cases 1 and 2, the deep base case with high GOR. Fig. 4 shows the relative change in the predicted volume median droplet size as a function of a relative change, over a realistic range, in each of four input variables, using the Johansen et al. (2013) coefficient values as the base prediction. For both the independent and dependent variables, the relative change is defined as (base case − perturbed case)/base case. The oil interfacial tension and the mass fluxes of gas and oil all have moderated influences on the results. Interfacial tension can produce changes of −36% and −51% to 40% and 61% over the range of realistic input values for cases with and without dispersant. The mass fluxes of oil and gas yield maximum changes between 40% and −30% to 20% and −36% independent of the use of dispersant. Meanwhile the dynamic viscosity becomes important only when adding dispersant, with the relative change ranging from −21% to 18%.

3.3. Intercomparison results

The initial droplet size distribution model sensitivity is explored further through analysis of the predictions submitted by the different teams in phase 1 of the model intercomparison exercise. Fig. 5 shows the equilibrium model results for the five teams who submitted data for the intercomparison along with predictions from the population dynamics model VDROP-J (not used by any of the integrated spill models, but shown for comparison). For the cases without dispersant (upper subplot in the figure for cases 1, 3 and 5), the predicted volume median diameters vary by factors of 5, 26 and 15, with values of the CV (computed from Eq. (5) with n = 6) of 52%, 76%, and 72%. For the cases with dispersant (lower subplot in the figure for cases 2, 4 and 6) the predicted diameters vary by factors of 8, 20 and 21, with CV values of 95%, 80%, and 65%. This spread in CV is changed to 36%, 61%, and 66% by removing the BLOSOM model, which assumed only a 30-fold reduction in interfacial tension compared to the 200-fold reduction assumed by the other models. The average CV using all six models is 73%, while for the five models using the same reduction in interfacial tension the average is 60%. Because there is uncertainty as to what the actual reduction in interfacial tension should be when adding different types of dispersants, at different temperatures, and using different injection techniques, the higher average is probably more realistic. As concerns the difference between equilibrium and population-based models, the results shown here for the asymptotic value at 100 m above the source for VDROP-J is within the range predicted by the equilibrium models. However, the size distribution evolves considerably from the source to its asymptotic value, and this variability is only captured by the population dynamics model (see e.g., Zhao et al., 2014b for further details of the evolution of the droplet size distribution).

The range in model predictions can be compared with the model uncertainty explored in the sensitivity studies discussed previously in connection with Fig. 3 through comparison of the respective values of the CV. The uncertainty among models (CV = 73%) is greater than the uncertainty in a given model using different calibration coefficients (CV = 27%), by a factor of 2.7, and greater than the uncertainty associated with oil properties (CV = 21%), by a factor of 3.5, suggesting the need for more model refinement and/or calibration. In this regard, we note that some of the smallest droplet sizes are predicted by the RSMAS model, whose model coefficients were calibrated to tank stirring tests of multiple crude oils dispersed in saltwater rather than jet breakup tests (Aman et al., 2015). On the other hand, other models (notably OILMAP DEEP for case 2) predicted smaller droplets than RSMAS as a result of differences in the oil equation-of-state. Moreover, Belore (2014) claim that the Johansen et al. (2013) and Brandvik et al. (2013a) coefficient values for Eq. (2) over-predict the droplet sizes for dispersant-treated cases compared to experiments at other facilities not included in their calibration datasets.

From both Figs. 3 and 5, it is evident that most of the predicted oil droplet sizes are in the range of 0.3–6 mm without the addition of dispersants, and that adding dispersants reduces the predicted droplet size to the range of 0.01–0.8 mm. It should be remembered that the models simulate the effect of dispersants by reducing the interfacial tension, so the models are only as good as their assumed values for IFT. To put these model predictions in context, Fig. 6 shows the model predictions together with much of the available laboratory and field data. The data are presented versus We^* using B_{50} = 0.8 as in Johansen et al. (2013). All of the laboratory data are for a single dispersed phase; the DeepSpill field experiment includes some data for a release of oil and gas. An important feature of the results for the API intercomparison cases is that they are all extrapolations beyond the range of measured data for this parameter space. It may be reasonable to assume that the scaling

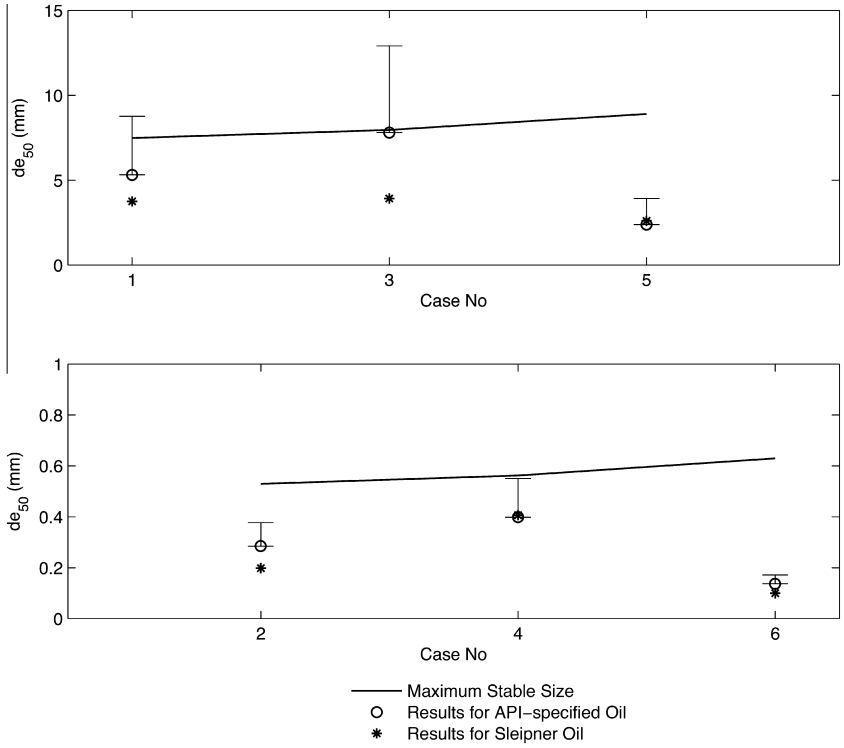

Fig. 3. Comparison of predictions for Eq. (2) for two different oils. Error bars show results for two sets of model coefficients.

laws (Eqs. (1) and (2)) extend beyond the laboratory scale, but no data are available to validate this assumption.

Although the modified Weber number model appears robust, there are several aspects that still require additional validation data. The models implicitly assume equilibrium, which may not be achieved until some distance from the release (Zhao et al., 2014a). Also, laboratory experiments with dispersants show that tip streaming in the presence of chemical dispersants may cause additional reduction in the droplet size, outside of the initial break-up regime close to the release (Gopalan and Katz, 2010; Nagamine, 2014). The lack of data with multiphase releases also makes it difficult to select an accurate method to predict droplet size for mixed gas and oil releases; the new data in (Belore, 2014) may help to bridge this gap. The effect of dispersant in reducing droplet size depends on knowing the effect of dispersant on reducing the interfacial tension and accurately modeling the limiting effect of viscosity. A constant reduction factor for surface tension with effective treatment has been used here, but this factor depends on the type of dispersant, its method of injection, and temperature. Finally, we note that only one modeling team applied the DSD model to predict the initial gas bubble size (OILMAP Deep, which predicted 4.4 mm for all cases). All others assumed the gas bubbles were initially 10 mm in diameter (the maximum stable bubble size for methane in seawater), and none of the teams assumed that dispersants would affect this initial gas bubble size. Since the gas bubbles are hydrocarbon mixtures, it is reasonable to assume that their interfacial tension would be reduced by chemical dispersants, and data is needed to quantify the efficiency of the reduction, which is significant for the rate of dissolution of the gas.

4. Nearfield plume

4.1. Comparison metrics

Nearfield plume models compute the evolution of their state space variables along the centerline trajectory of the plume by solving conservation equations for mass, momentum, energy, and concentration averaged over plume cross-sections. Multiphase components are included through force couplings between the droplet/bubble drag and the buoyant force on the entrained seawater. The discrete bubble model is used to account for dissolution: the dissolution of a single bubble or droplet is tracked along the plume trajectory and applied to a group of same-sized droplets/bubbles at the same point along the path. Equations for these models are summarized, for example, in Zheng et al. (2003), Johansen (2003), and Socolofsky et al. (2008).

Fig. 7a shows a schematic of a typical model prediction for an integral plume model with separation of gas bubbles and oil droplets in stratified crossflow. These models predict several state variables, and each implementation of the model in the intercomparison makes slightly different choices in the solution algorithm. We note that none of the models used in the intercomparison were capable of predicting multiple layers or subsurface intrusions. The parameters chosen for intercomparison are characteristic geometric and flow rate predictions of the model (e.g., trap height, entrained volume flow rate, gas mass flow rate, etc.). As depicted in the figure, the entrained seawater rises with the droplets and bubbles to a maximum height h_P before it is arrested by the stratification and starts to descend back toward a level of neutral buoyancy, where it forms an intrusion layer, which oscillates about the trap height h_T. If the crossflow is strong, the gas bubbles and possibly large oil droplets may leave the upstream side of the plume before reaching the height h_P; otherwise, most of the gas is expected to be in large enough bubbles that it would escape from the plume at h_P along with the larger oil droplets. Some small gas bubbles and oil droplets may continue to follow the entrained seawater into the intrusion layer. Ultimately, the simulation is stopped since the advection of the plume becomes nearly identical to the ambient currents. All gas bubbles or oil droplets either leaked from the edge of the plume or resident in the intrusion layer are passed to a farfield model, which tracks their on-going passive transport through the water column (see the following Section 5, below).

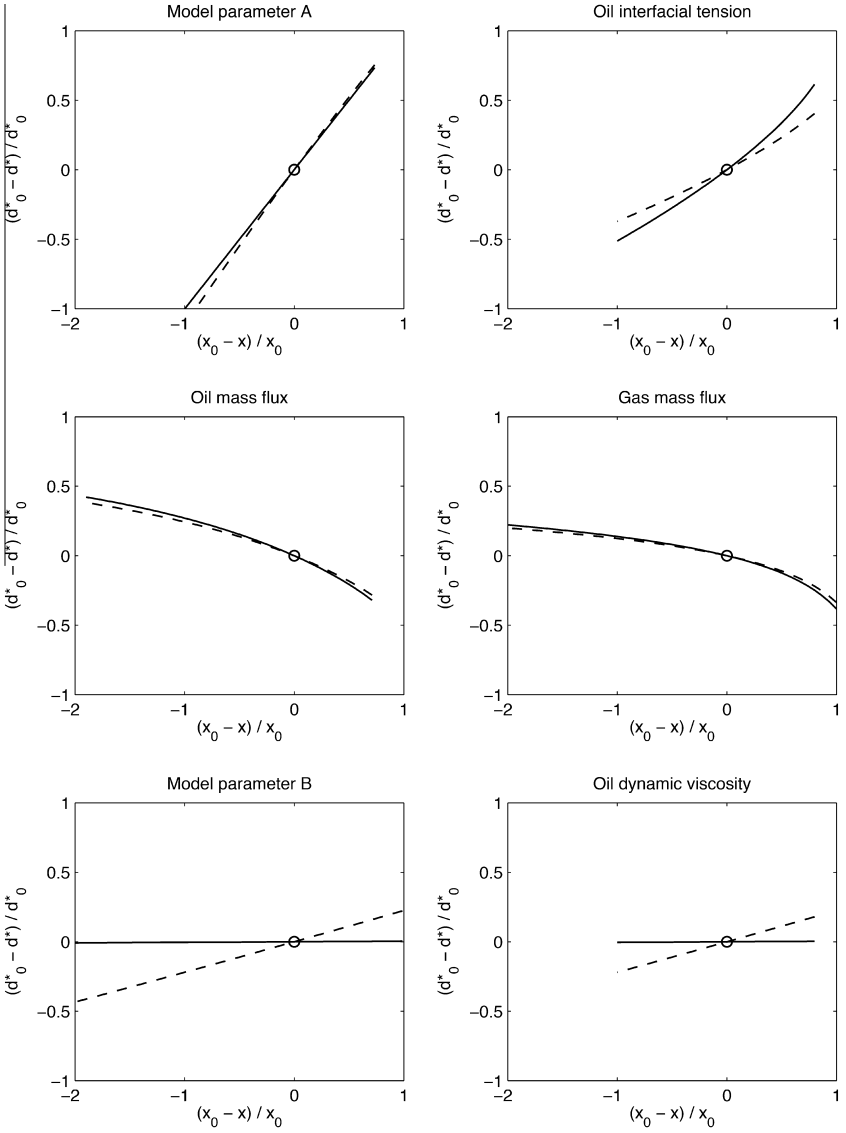

Fig. 4. Sensitivity analysis results for the breakup model Eq. (2). Solid line for test matrix case 1, the deep base case without dispersant; dashed line for test matrix case 2, the deep base case with dispersant. x and x_0 are the parameter values over a range and at their base-case values; d^* and d_0^* are the non-dimensional droplet size d_{50}/D over a range and at their base-case values.

Differences among model solution strategies largely are related to how the gas and large oil droplets leak from the upstream edge of the plume and where the plume-stage of the calculation is stopped. Laboratory data for the leakage of gas bubbles from the plume is available in Socolofsky and Adams (2002). The basic algorithm needed to match these data is a prediction of the bubble trajectory inside the plume, accounting for the entrainment velocity directed toward the plume centerline and the vertical slip velocity of the bubbles relative to the plume fluid velocity. OSCAR and MIKE by DHI OS module include a random motion algorithm for the gas bubbles and oil droplets within the plume; other models track the droplets and bubbles along deterministic trajectories.

There are three main choices used by modelers for deciding where to stop the nearfield plume calculations. The earliest choice is the location where the mixture density of the bubbles, droplets, and entrained plume fluid match the ambient density during the initial ascent of the plume. This is a neutral buoyancy level, and is close to the elevation of the trap height h_T. At this point along the plume trajectory, the plume contains excess momentum, and other models continue the simulation until the upward momentum decays to zero, which coincides with the high point h_P. Finally, some models continue the simulation farther, into the intrusion layer, stopping either after a couple of oscillations around h_T, when the last dispersed phase droplets leave the plume, or when the simulated plume velocity approaches the ambient velocity.

Each of the metrics used in the intercomparison is depicted in the Fig. 7a schematic. The geometric quantities include the separation height of gas on the upstream side of the plume h_S, the highest point along the plume trajectory h_P, and the intrusion depth h_T. The mass fluxes of gas leaving the plume at the separation height $\dot{m}_g$ and of oil leaving the plume at the maximum height $\dot{m}_o$ or entering the intrusion $\dot{m}_{oj}$ after the maximum height are key fluxes that can be compared. These help compare the way dissolution and separation are modeled for the gas and where the oil enters the farfield model (either at the maximum height or from the intrusion layer). The volume flux in the intrusion layer Q_i is important to predict dilution of dissolved hydrocarbons subsurface, and reflects differences in the entrainment or the termination point selected by each model. Hence, these bulk properties summarize the main

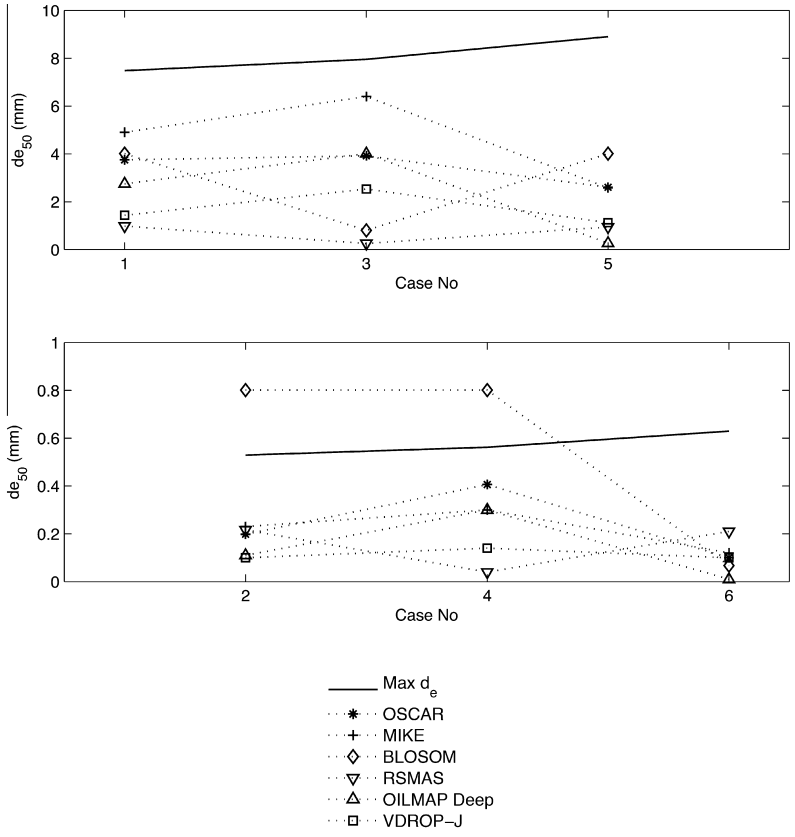

Fig. 5. Phase 1 results for droplet size prediction for test matrix cases 1 through 6.

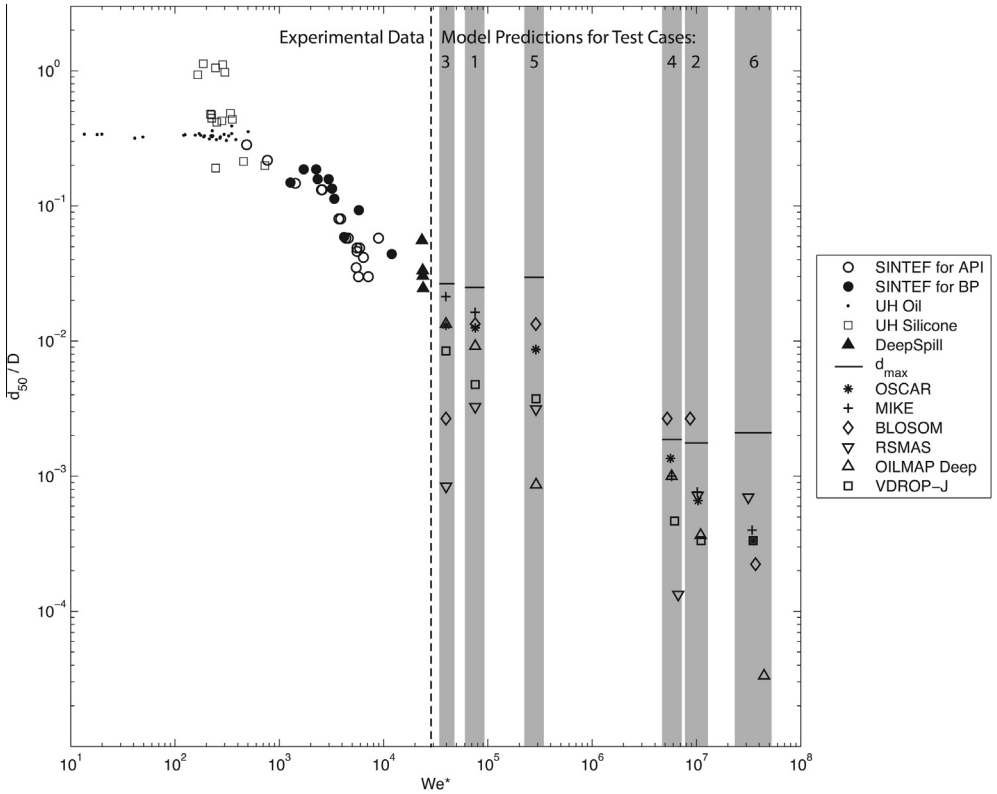

Fig. 6. Phase 1 modeling results for droplet size plotted together with the available observational data in non-dimensional space.

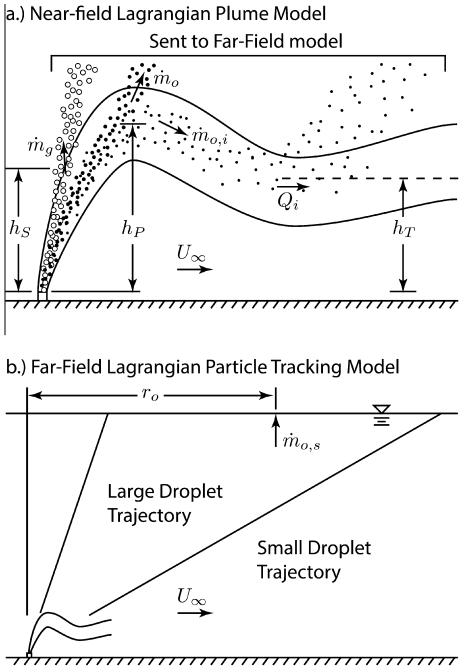

Fig. 7. Schematic of the nearfield plume models and farfield models indicating the locations of the metrics reported in the model intercomparison figures.

attributes of the plume solution, including differences in the model equations (e.g., how gas leaves the plume) and modeler choices (e.g., when to stop the nearfield solution).

4.2. Intercomparison results

Each of the metrics described above was compared among the participating models during the intercomparison. Here, we summarize a few key features of the intercomparison.

A fundamental property of a blowout plume is the formation of the subsurface intrusion layer, as observed extensively during the Deepwater Horizon accident (see e.g., Socolofsky et al., 2011; Spier et al., 2013). Fig. 8 shows the model predictions for the depth of the lowest intrusion layer, which is the depth corresponding to h_T in Fig. 7a. For all of the intercomparison figures, the upper subplot shows the deepwater cases, and the lower subplot summarizes the shallow tests cases; even-numbered case numbers are those treated with subsea chemical dispersant. In deep water, the predicted intrusion height has a mean value of 320 m above the bottom across all cases, with an average standard deviation among the model predictions of 105 m within each test case. For each modeling system, the trap depth remains fairly constant across test cases since the spill rate and stratification were similar in each case. As explained in Socolofsky and Adams (2005), trap height depends on buoyancy flux to the quarter power and stratification frequency to the three-quarter power. The stratification frequency was constant across all test cases, and the buoyancy flux varied primarily with the GOR. Cases 3 and 4 have lower trap depth for some models due to the lower GOR; case 7 has lower trap depth for some models due to the high crossflow yielding an earlier separation between the plume and gas bubbles.

The lower trap height estimates in Fig. 8 are for models that either terminate at the first occurrence of neutral buoyancy (i.e., before the maximum rise height in Fig. 7a), such as OILMAP Deep and MIKE by DHI OS module, or as a result of premature crossflow separation, such as BLOSOM. The values reported for CMS and LTRANS are for their initial conditions from the empirical equations in Socolofsky et al. (2011), which neglect the dissolution of gas and the forced entrainment due to the crossflow, thus, overestimating the buoyancy flux along the plume trajectory and yielding consistently higher trap heights. Cases 7 and 8 with high crossflow for CMS and LTRANS indicate that it is more the crossflow than the dissolution that is responsible for the higher values obtained through the empirical equations, which is consistent with the scaling laws being insensitive to buoyancy flux, which is removed by dissolution. Overall, these deepwater cases trap close to the release (320 m above bottom on average in 2000 m of water depth), so that the majority of the droplet rise (on average 85% in 2000 m depth of water) occurs in the farfield model.

The very low trap heights (between 3 and 50 m above the release) for BLOSOM in the shallow depth cases are due to the model incorrectly assuming the gas leaks out of the plume nearly immediately above the source; all other models predict plume surfacing for these shallow cases and no gas separation or subsurface intrusion formation.

Fig. 9 shows the volume flux of entrained seawater in the plume at the trap depth, which is the volume flux entering the intrusion layer. The values for this parameter depend on the entrainment model (and the selection of entrainment coefficient), and on the location along the plume centerline where the model is terminated. Entrainment models that include the crossflow (all models except the empirical equations for the initial conditions to CMS and LTRANS) will generally have higher volume fluxes. Likewise, models that terminate later will entrain more fluid. A common feature of the results is the prediction of a large intrusion layer flux, ranging from ~1000 to 5000 m^3/s (mean ~2000 m^3/s) which is within an order of magnitude of the flow of the Mississippi River as it enters the Gulf. This is a very significant flow rate, but it is distributed over a wide area at a level of neutral buoyancy, so that the intrusion velocity is only a few centimeters per second. Thus, the main utility of the intrusion layer flux is to evaluate the dilution of dissolved hydrocarbons leaving the plume and flowing into the intrusion layer. OSCAR and OILMAP Deep have similar values, with OILMAP Deep being generally lower since it terminates earlier along the plume centerline. CMS and LTRANS are consistently lower than OSCAR and OILMAP Deep since their equations neglect the enhanced entrainment from the crossflow. Only BLOSOM predicts an intrusion layer in the shallow cases, but as explained for Fig. 8, this was due to an error in predicting the gas separation from the plume. The range of variability for both the trap height (i.e., elevation above bottom) and intrusion flux are similar in relative differences, with scatter for both measures within about a factor of two of the mean values.

One major difference among these models as run for the intercomparison is how they handle the oil fate within the plume stage of the simulation. Few models, e.g., MIKE by DHI OS module and OSCAR, simulate dissolution in the nearfield plume, and only OSCAR simulates the plume trajectory into a few oscillations of the intrusion layer. OSCAR allows for larger droplets and gas bubbles to depart from the plume earlier than smaller droplets, and the intrusion layer contains both dissolved hydrocarbons as well as small droplets. Hence, the majority of the models predict the large and small oil droplets to enter the farfield together, either at the first neutral buoyancy level or the maximum rise height. The only way these models could predict hydrocarbon concentrations in the intrusion would be from dissolved hydrocarbon or if the droplets were small enough to continue downstream along the neutral buoyancy level. Observations during the Deepwater Horizon confirmed significant mass flux of heavier hydrocarbons in the intrusions (e.g., Spier et al., 2013), but none of the data can conclusively determine whether these concentrations are from dissolved or liquid oil.

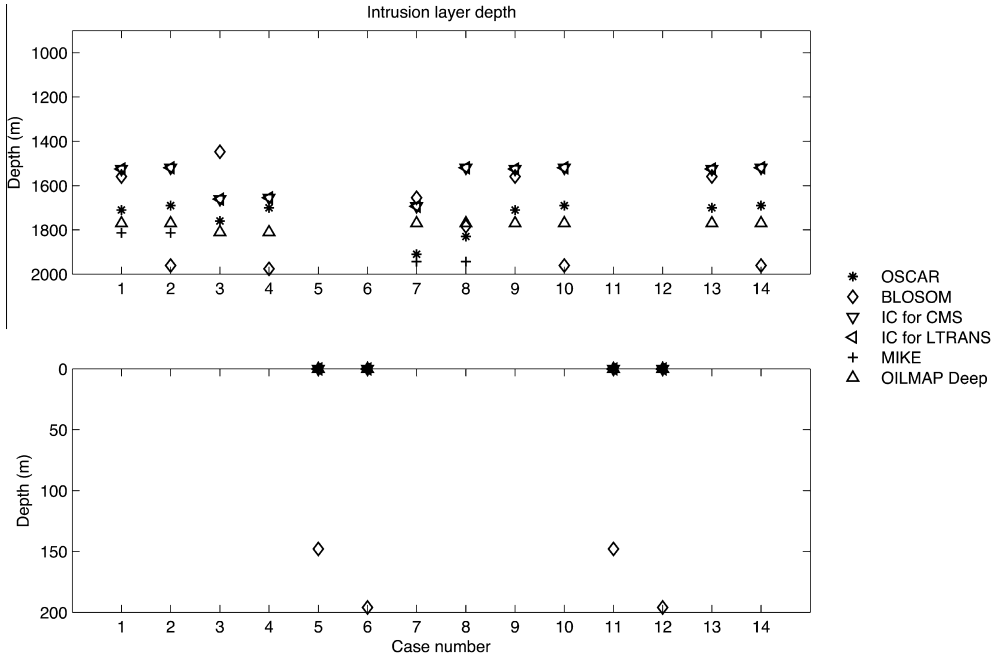

Fig. 8. Depth of the first intrusion layer above the release. Corresponds to the trap height h_T. Values reported with CMS and LTRANS are their initial conditions, computed from equations in Socolofsky et al. (2011).

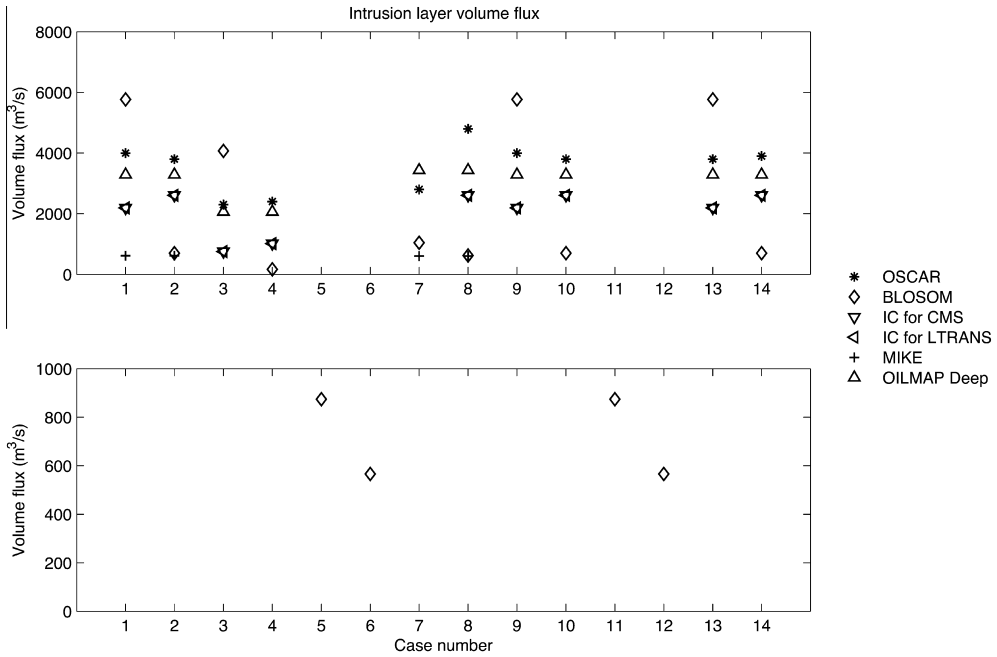

Fig. 9. Volume flux Q_i of entrained seawater predicted at the first intrusion layer above the release. Values reported with CMS and LTRANS are their initial conditions, computed from equations in Socolofsky et al. (2011).

Experiments by Chan et al. (2014) studied separation of large and small oil droplets at the intrusion using glass beads in an inverted frame of reference as a proxy for oil. These results were used in the correlation equations providing initial conditions to CMS and LTRANS. Fig. 10 shows the mass flux of oil entering the intrusion layer $\dot{m}_{oj}$ based on these correlation results along with the predictions from OSCAR, which does simulate oil transport to this region of the nearfield simulation. These two models receive the same inputs for all cases with the API-specified droplet sizes; only the modeler cases are different (cases 9 through 12), where CMS uses the droplet sizes from RSMAS in Fig. 5 and LTRANS uses the API-specified values corresponding to these cases. OSCAR and the LTRANS predictions are in strong agreement across all cases. We note that none of the data from Chan et al., 2014 were available to OSCAR; hence, the physics represented in OSCAR for bubble and droplet separation based on Socolofsky and Adams (2002) appears robust. The no-dispersant case 9 using the modelers' droplet size for CMS predicts significantly more oil in the intrusion than either OSCAR or the predictions for LTRANS; hence, the small droplet sizes in the no-dispersant cases

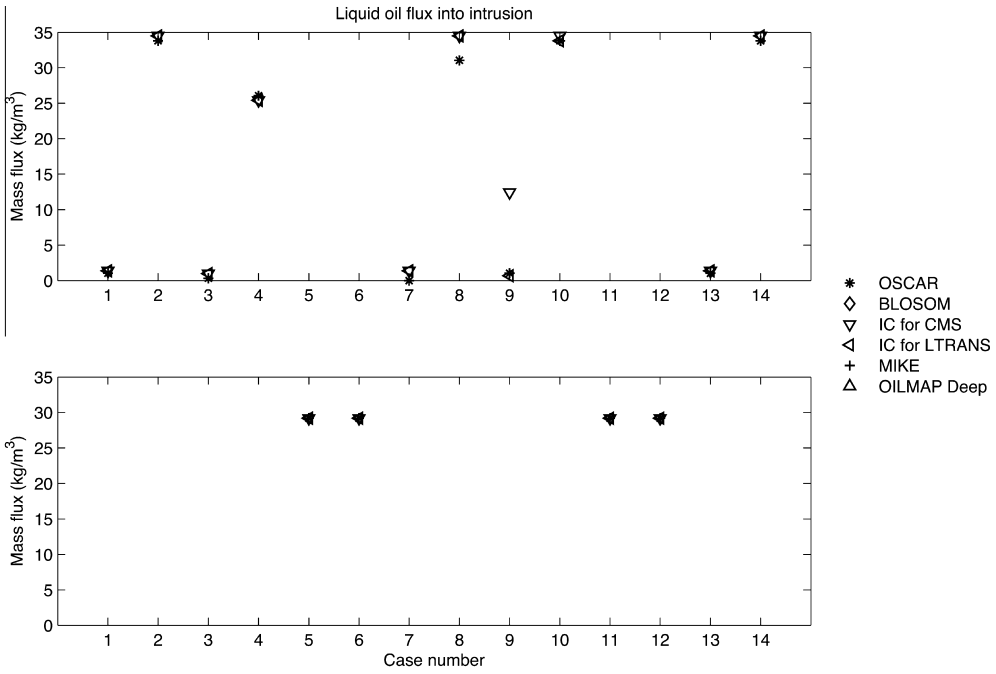

Fig. 10. Mass flux $\dot{m}_{o,j}$ of oil entering the intrusion layer. Values reported with CMS and LTRANS are their initial conditions, computed from equations in Chan et al. (2014).

predicted by RSMAS are small enough to show significant intrusion without dispersant addition. This is consistent with the results in Paris et al. (2012) and is a result of their smaller predicted droplet sizes (Adams et al., 2013). In the shallow cases, all models predict the full oil mass flux to reach the surface and enter the surface intrusion.

These intercomparison data demonstrate the variability among nearfield model predictions for the fate of oil and gas in the plume stage of transport. In deepwater, the trap height predictions are between 50 and 500 m above bottom and the intrusion layer flux is in the range of 1000–5000 m^3/s, depending on the GOR, cross-flow speed, and ambient stratification. Model predictions for the trap heights and fluxes of entrained water into the intrusion layer are of a similar order of magnitude for each metric across all models, with variability spanning about a factor of two for each test case. Much of this variability is operational, depending on where the modeler chooses to stop the nearfield simulation, rather than a result of different model calibration or validation. However, some of the newer models do contain errors (e.g., premature gas separation from the plume in the BLOSOM model). Some models distinguish between oil that flows out at the maximum height of rise of the plume and oil that enters the intrusion, while other models pass oil droplets to the far field at a single trapping height. In either case, the altitude where the oil will be passed to the Lagrangian model is similar, with the main difference being the downstream distance at which this takes place. How each of these differences affects the ultimate fate of the oil in the water column requires consideration of the Lagrangian particle-tracking phase of the transport.

5. Farfield Lagrangian tracking

5.1. Comparison metrics

The farfield models receive the bubbles and droplets from the end of the nearfield plume simulation and track their motion through the water column. In addition to advection by ambient currents, and buoyant rise, farfield models almost always include a random motion to account for horizontal and vertical diffusion. In addition, many models simulate oil fate processes. Some include dissolution and most include a first-order rate loss to model biodegradation, with more complicated models using different rates for different components of the oil. Farfield models necessarily have large domains, and in real events, require specification of the full three-dimensional velocity field; hence, they are generally coupled to computational fluid dynamic (CFD) circulation models of the ambient currents. For the intercomparison, the current velocities were simplified to be uniform and steady over the water depth so that coupling to CFD simulations was not required. Indeed, in the case of constant horizontal and vertical eddy diffusivity, the farfield solution can be obtained analytically for these test cases.

Fig. 7b shows a schematic of the farfield simulation domain for a typical deepwater case, including a depiction of the nearfield plume providing the initial conditions. The figure is not to scale, but the relative distances along the plume trajectory and farfield simulation for a deepwater blowout (e.g., the 2000 m depth cases) is representative of a real simulation: ~85% of the vertical transport from this depth occurs in the farfield. Larger bubbles and droplets surface closer to the source, while smaller ones take longer to rise, surfacing farther downstream. In the simulations presented here, the bubble and droplet size distributions are modeled using a range of sizes taken from the size distributions; thus, the center of the surfacing zone lies between the locations where the largest and smallest droplets/bubbles surface. The distance to this center of the surfacing zone for oil is depicted as r_o in the figure. The mass flux of oil to the sea surface integrated over the entire surfacing zone is $\dot{m}_{o,s}$. Since the forcing is steady, at steady state and neglecting dissolution and biodegradation, $\dot{m}_{o,s}$ will converge to the inflow rate of oil at the release, which is 20,000 bpd in each of the test cases. Reaching steady state can take considerable time, especially in the cases with dispersant, and all results presented here are calculated after 14 days of simulation time.

5.2. Intercomparison results

Fig. 11 presents the model results for the downstream distance to the center of mass of the surfacing zone for each of the test

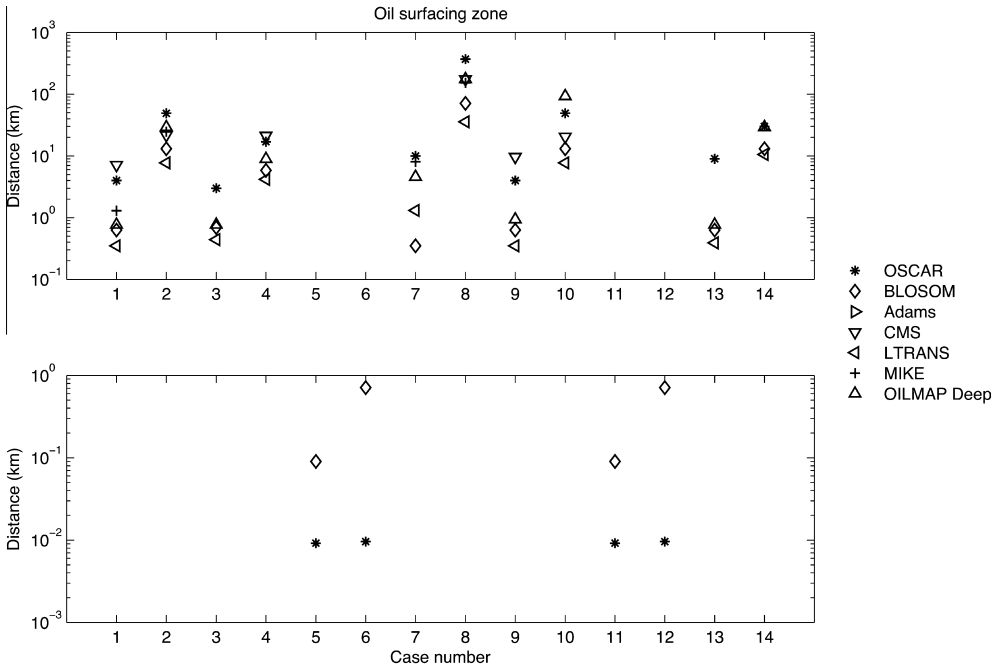

Fig. 11. Distance r_0 from the release point to the downstream center of the surfacing zone.

cases, and Fig. 12 presents the oil mass flux through the surfacing zone. Since the farfield forcing is a uniform and steady crossflow, differences among models largely reflect the different initial conditions obtained from the nearfield simulations and the degradation processes modeled in the farfield. While the selection of the horizontal eddy diffusivity also influences the results, the center of the surfacing zone and mass flux to the surface should be insensitive to this spreading parameter for a uniform, steady current. In the cases where the modelers use their own size distributions (cases 9 through 12), differences for droplet size may also be significant.

For the shallow water cases (5, 6, 11, and 12), OSCAR's surface resuspension plume can be compared to the BLOSOM results with premature gas separation. In OSCAR the oil reaches the surface almost immediately via the plume; BLOSOM predicts oil surfacing over an order of magnitude farther downstream since it simulates the oil rise passively (i.e., outside the plume) over the majority of the water column. This highlights the importance of the rising plume in shallow water and near the blowout source.

In deep water, Fig. 11 shows that models predict that the reduction of interfacial tension by dispersants (odd numbered cases) shifts the surfacing zone further downstream compared to the

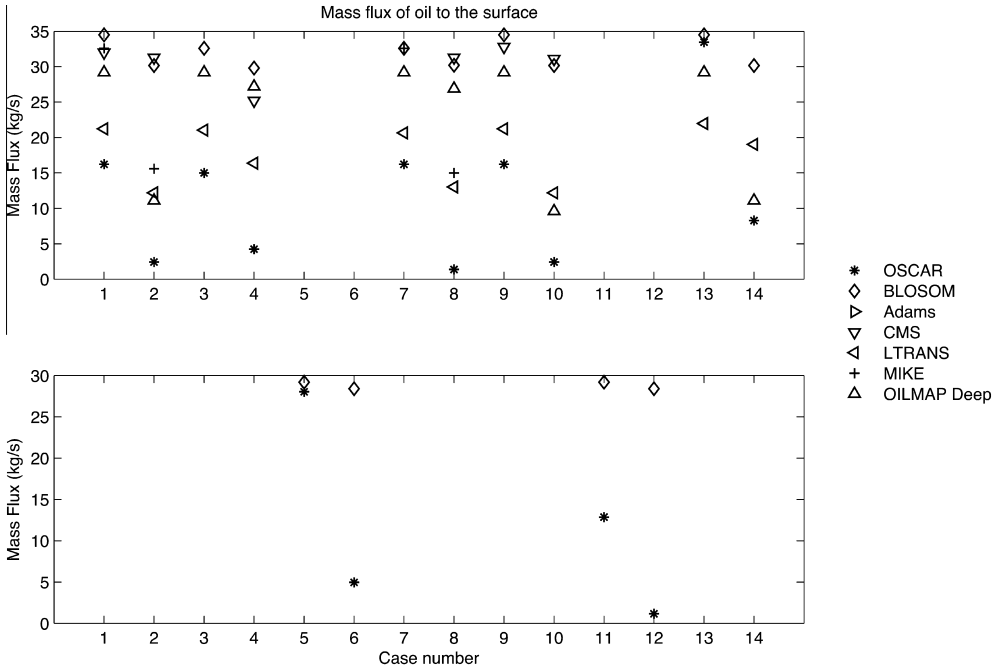

Fig. 12. Mass flux $\dot{m}_{o,s}$ of oil integrated over the surfacing zone.

no-dispersant cases (even numbers), by factors ranging from 2.1 to 202. Averaged over the 5 pairs of cases and up to 6 different models, the average ratio of the surfacing distances with to without dispersants was 29. For a given case, there is also substantial variability among predicted surfacing distances. The coefficient of variation for the surfacing distance are 114%, 97%, 86%, 126% and 156% for cases 1, 3, 7, 9, and 13 without dispersant and 60%, 64%, 71%, 96% and 50% for cases 2, 4, 8, 10, and 14 with dispersant. For the no-dispersant cases, the downstream surfacing distance varies among models by a factor of 27 (from 0.35 to 9.6 km) in the low currents and by a factor of 29 (0.35–10 km) in the high current cases. When subsurface dispersants are applied, the downstream surfacing distance varies by a factor of 12 (from 7.7 to 93 km) in the low crossflow cases and by a factor of 10 (36–370 km) in the high crossflow cases. OSCAR generally predicts surfacing to occur farthest downstream. The distances are farther in OSCAR because the nearfield plume extends into the intrusion layer and dissolution and biodegradation were included for all test cases run except 13 and 14. For case 10, the ASA OILMAP DEEP model predicts a farther downstream surfacing zone because they assumed smaller droplets in their own size distribution. For the cases where CMS predicts farther downstream surfacing, they simulated a smaller median droplet size at the source. Together, these results highlight the predicted hydrodynamic effect of subsurface dispersant injection for deepwater cases: the predicted surfacing zone moves significantly downstream when subsea dispersants are used when compared to the no-dispersant cases.

The oil mass flux to the surfacing zone is depicted in Fig. 12, and largely reflects the different equations of state and dissolution and degradation processes and rates used in each model. The different equations of state result in oil fluxes between 27 and 35 kg/s; hence, models predicting surfacing fluxes in these ranges generally predict 100% of the oil coming to the surface. Lower oil surfacing fluxes either result from dissolution and biodegradation (e.g., OSCAR or LTRANS) or from a large quantity of small droplets that have not yet surfaced at the end of the simulation (e.g., OILMAP DEEP, CMS). OSCAR predicts generally the lowest fluxes since it simulates oil dissolution and degradation in all cases except 13 and 14; whereas, LTRANS was the only other models to consider oil degradation for any of the cases. Temperature- and fraction-dependent biodegradation described in CMS (Paris et al., 2012; Lindo-Atichati et al., 2014) were turned off for simplification of comparison. LTRANS uses first-order decay with an average half-life of 3.05 days, and the empirical initial conditions provided to LTRANS via the trap height were consistently higher in the water column than predicted by the other models. Differences among models in the assumed vertical diffusion parameter will also affect surfacing; however, all models assume droplets continuously rise at their predicted slip velocity. The wide spread in predictions for oil mass flux indicates that it is sensitive to the oil equation of state, the initial droplet size distribution, the location of the nearfield initial conditions, and the rates of dissolution and biodegradation.

Despite this spread in predictions, a few trends are consistent among the models. One important result here relates to the fraction of the released oil that reaches the surface in the deepwater simulations. In the absence of degradation, most of the oil reaches the surface within the 14 day simulation period. The exceptions are a few dispersant cases with very small oil droplets, such as case for OILMAP Deep, where over 30% of the oil still surfaces. Thus, without degradation, most model results for this blowout condition suggest it is difficult to generate droplet sizes that are small enough to remain sequestered over 14 days whether subsea dispersant is applied or not. When biodegradation and dissolution are added, OSCAR and LTRANS predict a lower surface flux. Without dispersant, about half of the light oil released in these test scenarios is predicted by OSCAR to surface. When dispersant is added, the more efficient dissolution and biodegradation afforded by the smaller droplets, with larger surface areas and their slower rise velocities, result in a significant reduction in the surface flux, with up to 95% of the released oil mass failing to reach the surface (e.g., case 8 with large currents). Hence, most models predict that dispersants increase both the downstream distance where surfacing occurs and the rates of dissolution, degradation, and suspension occurring in the water column.

For the shallow scenarios, the oil is transported directly to the surface because of the gas buoyancy and very little is degraded before surfacing. A key concern in this case is the flux of gas to the surface since this presents a potential explosion hazard. Both OSCAR and OILMAP Deep predict gas fluxes of ~5 kg/s to the surface in cases 5, 6, 11 and 12. This is a little less than half of the released gas, and represents a significant surface hazard; other models did not report this metric. Hence, it is important to evaluate the response zone conditions in shallow water whether subsea dispersant is added or not. In these cases, one reason to inject subsurface dispersant would be to localize the dispersant addition with the expectation that it would reduce the need for airborne dispersant addition in the farfield. One could expect that oil, treated with subsurface dispersant, would be more easily redispersed (entrained) once it surfaced as long as the active ingredient of the dispersant does not leach out during the rise to the surface. For the shallow cases, rise time is very short, and it can be expected that treated oil will end up on the surface; indeed, this effect is seen in the OSCAR predictions, where the low surface flux of oil in cases 6 and 12 are due to suspension of small oil droplets in the water column. Whether or not oil that is treated subsurface is indeed more readily dispersed once it surfaces, however, requires testing.

In addition, as noted, all the models assumed that dispersant would have no influence on the gas bubble size distributions. As described, it is reasonable to assume that surfactants would reduce the interfacial tension of the hydrocarbon gas. If this is the case, gas bubble sizes would be reduced, and this in turn would reduce the bubble rise velocity and increase the rate of dissolution, thus reducing the buoyancy of the entire plume and the gas flux at the surface. Additional research is also needed to determine the extent that dispersants influence gas bubble sizes.

6. Summary and conclusions

In this paper we have defined a set of 14 test cases of accidental oil well blowouts in shallow and deep water, with and without subsea chemical dispersant application, where the effect of the dispersant has been simulated through a reduction in the oil–water interfacial tension. We present the predictions for several key metrics from a set of mainstream and research models for each of these cases. The models each consist of three sequential steps, including prediction of the initial bubble and droplet size distribution, simulation of oil and gas through a nearfield plume model, and tracking of the farfield transport of oil and gas in a Lagrangian particle tracking phase. The models all make different assumptions about some of the input parameters and include different solution strategies, and differences among model predictions reflect this variability.

For the prototype blowout (with an oil flow rate 1/3 that of the Deepwter Horizon), models predict volume median droplet sizes of about 0.3–6 mm without dispersant and 0.01–0.8 mm with dispersant. Simulation differences result from different empirical model fit coefficients, different assumptions regarding the oil equation of state, and different ways of handling gas and oil mixtures; for the models used here the average CV of the predictions was 73%.

We note that there is a wide range of small-scale laboratory data but limited field data available for model validation, and all 14 cases of the model intercomparison lie outside of the non-dimensional parameter space covered by the observations. Hence, the application of empirical models for the equilibrium bubble and droplet size distributions are extrapolations beyond measured data, and rely on preservation of the dominant physics to larger scales. Sensitivity studies showed that model variability due to the range of calibration parameters had a CV of 27%, similar to the variability due to analysis using oil with slightly different properties (CV = 21%), but significantly less than the variability among models (average CV of 73%). Other sensitivity studies explored a more complete range of model parameters. The addition of chemical dispersants at the source was estimated to yield a 200-fold reduction on the interfacial tension between oil and water, producing a reduction in droplet size of at least an order-of-magnitude for the cases studied here. There is limited data for multiphase breakup (e.g., oil and gas), and each model handles the multiphase problem differently. Hence, to improve the assessment of model performance, observations at larger scale and with multiphase releases are needed.

Each of the nearfield plume models presented in the intercomparison were of the Lagrangian integral plume type, and most predicted a single intrusion layer a few 100 m above the release. The height of the intrusion formation depended partly on the simulation approach, with models that terminate at neutral buoyancy level generally in agreement and models that terminate at the maximum plume rise generally predicting a higher intrusion layer height. The extra entrainment caused by the crossflow also lowers the intrusion layer depth relative to predictions that ignore the crossflow. Indeed, the intrusion layer depth is more sensitive to the entrainment model than to the buoyancy flux (release flux) or oil equation of state. For the deepwater cases, models predict a range in intrusion flows between $\sim$1000 m^3/s and $\sim$5000 m^3/s (mean of $\sim$2000 m^3/s). Most models were in agreement that hydrocarbons released in the shallow cases propagate directly to the sea surface; exceptions occur when the numerical method incorrectly separates the plume from the gas prematurely. The plume model predictions for all of these parameters were largely insensitive to droplet size distribution within the range of droplets simulated by each model. While the plume stage of transport was relatively small in the deepwater cases simulated here (up to 500 m out of 2000 m depth), this stage was 100% of transport in the shallow cases, and can be significant for accidents in less than 2000 m depth of water.

For the first two stages of transport (initial droplet size prediction and trap height), the models generally agreed to within an order of magnitude. Predicted volume median droplet sizes varied by a factor of 5–26 with an average CV = 73%, while predicted trap height varied by a factor of ten (50–500 m). Prediction differences within the farfield were somewhat larger, reflecting the cumulative effects of differences in simulated droplet size and nearfield plume behavior in addition to farfield transport. For simulated distances to the downstream surfacing zone, model predictions varied by factors of 2.8–29 depending for high and low current speeds with and without dispersants. Models predicting early surfacing generally had higher trap heights, neglected dissolution and biodegradation, or assumed larger droplet sizes; models predicting larger distances to surfacing generally included dissolution and biodegradation and/or assumed smaller droplets. For the mass flux to the surfacing zone, the model predictions were also variable. While model predictions were consistent with the modeling choices (e.g., we do not suspect modeling errors), a consensus did not emerge for that metric due to the wide range of modeling choices that were made owing to the *pro bono* nature of the intercomparison (e.g., those neglecting dissolution and degradation predicted most of the oil to surface but under different equations of state, and those modeling fate processes used different algorithms and rates).

Despite these challenges, two model predictions were consistent within each modeling platform, and these are significant for future response, spill preparedness, and planning. First, in cases with subsurface dispersant addition, the smaller oil droplets were predicted to surface an order of magnitude farther downstream than for the untreated cases: 100's of meters become kilometers and kilometers become 10's of kilometers. Second, in cases with subsurface dispersant, much less oil is predicted to reach the surface, with oil either remaining suspended in the water column or being dissolved and biodegraded during transit to the surface. When degradation processes are considered, the smaller droplets dissolved and degraded much faster than untreated, larger droplets due to their higher surface area to volume ratio and longer rise time; in simulations with fate processes included, up to 95% of the released oil is predicted to fail to surface within 14 days of release in the high crossflow cases. Hence, the outcome of these simulations is a consensus that subsea dispersant addition moves the surfacing zone downstream by an order of magnitude beyond that for untreated cases and can result in a significant fraction of the released oil never reaching the sea surface.

This intercomparison included several of the more commonly used integrated spill models. While the models agreed reasonably well with each other in many respects, they differed in other respects by an order of magnitude or more. This variability points to the need for new models, new validation data, and perhaps new ways to interpret data. As examples, each model predicts a characteristic droplet size assuming equilibrium turbulence and Weber or modified Weber number scaling, based on source conditions. Such models should be compared with the class of dynamic models that predict the evolution of droplet sizes based on time-varying break-up and coalescence. Furthermore, all droplet size models were calibrated to laboratory or small scale field experiments, and then had to be extrapolated to field conditions; there is a need for additional experimental data that extends to the non-dimensional space of real field-scale releases. Models would also benefit from data involving release of both oil and gas. At the plume scale, all models were of the Lagrangian integral type allowing for a single subsurface intrusion. For the plume stage, it is unknown under what field conditions multiple intrusion layers will form. For the Deepwater Horizon accident, a few subsurface intrusions were documented (Spier et al., 2013). If a plume-stage persists above the first intrusion, oil will rise more rapidly through the water column and may surface closer to the release point, yet none of the models here considered multiple intrusions. For these reasons, additional experiments on plume behavior above the first intrusion are needed. For the farfield simulations, droplet size becomes more important than in the nearfield plume, and dissolution and biodegradation play a key role in the oil fate. Differences in how the models handled these processes in this intercomparison yielded predictions for surfacing metrics that spanned an order of magnitude. The farfield simulations were quite simple here, with a uniform and steady crossflow, and one could imagine that more realistic flow conditions would accentuate model differences even further. Hence, especially in deepwater, where farfield transport can be significant, initial oil droplet size distribution and the rates of the fate processes are critical to improving confidence in model predictions.

Acknowledgements

The modeling runs summarized in the paper figures were conducted *pro bono* by each of the modeling teams. The model intercomparison workshop and the analysis of the model results was

supported jointly by the API Joint Industry Task Force D3 Subsurface Dispersant Injection team and by the BP/Gulf of Mexico Research Initiative through the Gulf Integrated Spill Response (GISR) and Center for Integrated Modeling and Analysis of the Gulf Ecosystem (C-IMAGE) consortia.

References

Adams, E.E., Socolofsky, S.A., Boufadel, M., 2013. Comment on "Evolution of the Macondo Well Blowout: Simulating the Effects of the Circulation and Synthetic Dispersants on the Subsea Oil Transport". Environ. Sci. Technol. 47 (20). http://dx.doi.org/10.1021/es4034099 (11905–11905).

Aman, Z.M., Paris, C.B., May, E.F., Johns, M.L., Lindo-Atichati, D., 2015. High-pressure visual experimental studies of oil-in-water dispersion droplet size. Chem. Eng. Sci. 127, 392–400. http://dx.doi.org/10.1016/j.ces.2015.01.058.

Asaeda, T., Imberger, J., 1993. Structure of bubble plumes in linearly stratified environments. J. Fluid Mech. 249, 35–57.

Bandara, U.C., Yapa, P.D., 2011. Bubble sizes, breakup, and coalescence in deepwater gas/oil plumes. J. Hydraul. Eng. – ASCE 137 (7), 729–738. http://dx.doi.org/10.1061/(asce)hy.1943-7900.0000380.

Belore, R., 2014. Subsea chemical dispersant research. In: Paper Presented at Proceedings of the 37th AMOP Technical Seminar on Environmental contamination and Response, Environment Canada, Canmore, Alberta, Canada.

Brandvik, P.J., Johansen, Ø., Farooq, U., Angell, G., Leirvik, F., 2013a. Sub-surface oil releases – experimental study of droplet distributions and different disperant injection techniques. A scaled experimental approach using the SINTEF Tower Basin. *Rep.*, Prepared by SINTEF Materials and Chemistry, Trondheim, Norway.

Brandvik, P.J., Johansen, Ø., Leirvik, F., Farooq, U., Daling, P.S., 2013b. Droplet breakup in subsurface oil releases – Part 1: Experimental study of droplet breakup and effectiveness of dispersant injection. Mar. Pollut. Bull. 73 (1), 319–326. http://dx.doi.org/10.1016/j.marpolbul.2013.05.020.

Chan, G.K.Y., Chow, A.C., Adams, E.E., 2014. Effects of droplet size on intrusion of sub-surface oil spills. Environ. Fluid Mech. (in preparation)

Chen, F.H., Yapa, P.D., 2003. A model for simulating deepwater oil and gas blowouts – Part II: Comparison of numerical simulations with "deepspill" field experiments. J. Hydraul. Res. 41 (4), 353–365.

Chen, F.H., Yapa, P.D., 2007. Estimating the oil droplet size distributions in deepwater oil spills. J. Hydraul. Eng. – ASCE 133 (2), 197–207.

Clift, R., Grace, J., Weber, M.E., 1978. Bubbles, Drops, and Particles. Dover Publications Inc., Mineola, New York.

Gopalan, B., Katz, J., 2010. Turbulent shearing of crude oil mixed with dispersants generates long microthreads and microdroplets. Phys. Rev. Lett. 104 (5), 4. http://dx.doi.org/10.1103/PhysRevLett.104.054501.

Hinze, J.O., 1955. Fundamentals of the hydrodynamic mechanism of splitting in dispersion processes. AIChE J. 1 (3), 289–295. http://dx.doi.org/10.1002/aic.690010303.

Jirka, G.H., 2004. Integral model for turbulent buoyant jets in unbounded stratified flows. Part I: Single round jet. Environ. Fluid Mech. 4 (1), 1–56.

Johansen, O., 2000. DeepBlow – a Lagrangian plume model for deep water blowouts. Spill Sci. Technol. Bull. 6 (2), 103–111.

Johansen, O., 2003. Development and verification of deep-water blowout models. Mar. Pollut. Bull. 47 (9–12), 360–368. http://dx.doi.org/10.1016/s0025-326x(03)00202-9.

Johansen, O., Rye, H., Cooper, C., 2003. DeepSpill – field study of a simulated oil and gas blowout in deep water. Spill Sci. Technol. Bull. 8 (5–6), 433–443. http://dx.doi.org/10.1016/s1353-2561(02)00123-8.

Johansen, O., Brandvik, P.J., Farooq, U., 2013. Droplet breakup in subsea oil releases – Part 2: Predictions of droplet size distributions with and without injection of chemical dispersants. Mar. Pollut. Bull. 73 (1), 327–335. http://dx.doi.org/10.1016/j.marpolbul.2013.04.012.

Lee, J.H.W., Chu, V.H., 2003. Turbulent Jets and Plumes: A Lagrangian Approach. Kluwer Academic Publishers Group, Dordrecht, The Netherlands.

Levitus, S., Boyer, T.P., Conkright, M.E., O'Brien, T., Antonov, J., Stephens, C., Stathoplos, L., Johnson, D., Gelfeld, R., 1998. World Ocean Database 1998, vol 1: Introduction. NOAA NESDIS, Washington, D.C.

Lindo-Atichati, D., Paris, C.B., Le Hénaff, M., Schedler, M., Valladares Juárez, A.G., Müller, R., 2014. Simulating the effects of droplet size, high-pressure biodegradation, and variable flow rate on the subsea evolution of deep plumes from the Macondo blowout. Deep Sea Res. Part II (0). http://dx.doi.org/10.1016/j.dsr2.2014.01.011.

McCain Jr., W.D., 1990. The Properties of Petroleum Fluids, second ed. PennWell Publishing Company, Tulsa, Oklahoma.

McNutt, M.K., Camilli, R., Crone, T.J., Guthrie, G.D., Hsieh, P.A., Ryerson, T.B., Savas, O., Shaffer, F., 2011. Review of flow rate estimates of the Deepwater Horizon oil spill. Proc. Natl. Acad. Sci. http://dx.doi.org/10.1073/pnas.1112139108.

Nagamine, S. I., 2014. The effects of chemical dispersants on buoyant oil droplets, MSc. Thesis, Department of Mechanical Engineering, U. Hawaii at Manoa.

Paris, C.B., Hénaff, M.L., Aman, Z.M., Subramaniam, A., Helgers, J., Wang, D.-P., Kourafalou, V.H., Srinivasan, A., 2012. Evolution of the Macondo well blowout: simulating the effects of the circulation and synthetic dispersants on the subsea oil transport. Environ. Sci. Technol. 46 (24), 13293–13302. http://dx.doi.org/10.1021/es303197h.

Sarmiento, J.L., Gruber, N., 2006. Ocean Biogeochemical Dynamics. Princeton University Press, Princeton, NJ.

Seol, D.-G., Bryant, D.B., Socolofsky, S.A., 2009. Measurement of behavioral properties of entrained ambient water in a stratified bubble plume. J. Hydraul. Eng. – ASCE 135 (11), 983–988.

Socolofsky, S.A., Adams, E.E., 2002. Multi-phase plumes in uniform and stratified crossflow. J. Hydraul. Res. 40 (6), 661–672.

Socolofsky, S.A., Adams, E.E., 2005. Role of slip velocity in the behavior of stratified multiphase plumes. J. Hydraul. Eng. – ASCE 131 (4), 273–282.

Socolofsky, S.A., Bhaumik, T., Seol, D.G., 2008. Double-plume integral models for near-field mixing in multiphase plumes. J. Hydraul. Eng. – ASCE 134 (6), 772–783.

Socolofsky, S.A., Adams, E.E., Sherwood, C.R., 2011. Formation dynamics of subsurface hydrocarbon intrusions following the Deepwater Horizon blowout. Geophys. Res. Lett. 38, L09602. http://dx.doi.org/10.1029/2011GL047174.

Spier, C., Stringfellow, W.T., Hazen, T.C., Conrad, M., 2013. Distribution of hydrocarbons released during the 2010 MC252 oil spill in deep offshore waters. Environ. Pollut. 173, 224–230. http://dx.doi.org/10.1016/j.envpol.2012.10.019.

Tsouris, C., Tavlarides, L.L., 1995. Breakage and coalescence models for drops in turbulent dispersions (vol 40, pg 395, 1994). AIChE J. 41 (8) (1851–1851).

Valentine, D.L. et al., 2010. Propane respiration jump-starts microbial response to a deep oil spill. Science 330 (6001), 208–211. http://dx.doi.org/10.1126/science.1196830.

Wang, C.Y., Calabrese, R.V., 1986. Drop breakup in turbulent stirred-tank contactors. Part II: Relative influence of viscosity and interfacial tension. AIChE J. 32 (4), 667–676. http://dx.doi.org/10.1002/aic.690320417.

Zhao, L., Boufadel, M.C., Socolofsky, S.A., Adams, E., King, T., Lee, K., 2014a. Evolution of droplets in subsea oil and gas blowouts: Development and validation of the numerical model VDROP-J. Mar. Pollut. Bull. 83 (1), 58–69. http://dx.doi.org/10.1016/j.marpolbul.2014.04.020.

Zhao, L., Torlapati, J., Boufadel, M.C., King, T., Robinson, B., Lee, K., 2014b. VDROP: a comprehensive model for droplet formation of oils and gases in liquids – incorporation of the interfacial tension and droplet viscosity. Chem. Eng. J. 253, 93–106. http://dx.doi.org/10.1016/j.cej.2014.04.082.

Zheng, L., Yapa, P.D., Chen, F.H., 2003. A model for simulating deepwater oil and gas blowouts – Part I: Theory and model formulation. J. Hydraul. Res. 41 (4), 339–351.